J. Fluid Mech. (2024), *vol*. 978, A3, doi:10.1017/jfm.2023.1001

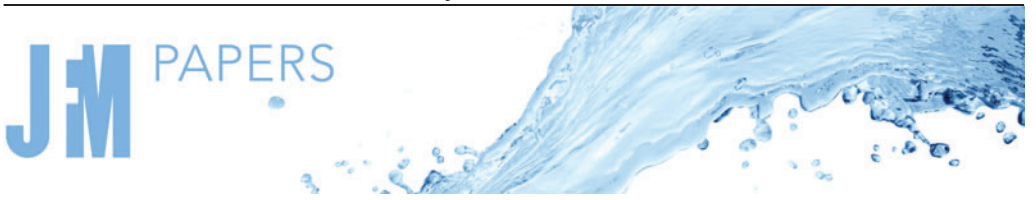

On local isotropy and scale dependence of pair dispersion in turbulent canopy flows

Ron Shnapp[1],†, Alex Liberzon[2], Yardena Bohbot-Raviv[3] and Eyal Fattal[3]

[1]Mechanical Engineering Department, Ben Gurion University of the Negev, POB 653, Beer Sheva 8410501, Israel

[2]School of Mechanical Engineering, Tel Aviv University, POB 39040, Tel Aviv 6997801, Israel

[3]Israel Institute for Biological Research, POB 19, Ness Ziona 7410001, Israel

(Received 10 June 2023; revised 28 September 2023; accepted 22 November 2023)

Canopy flows in the atmospheric surface layer play important economic and ecological roles, governing the dispersion of passive scalars in the environment. The interaction of high-velocity fluid and large-scale surface-mounted obstacles in canopy flows produces drag and causes intense, inhomogeneous and anisotropic turbulence. In this work, we focus on the turbulent dispersion of passive scalars by studying the 'pair dispersion' – a statistical measure of relative motion between particles. We analyse the results of a three-dimensional particle tracking velocimetry experiment in a wind-tunnel canopy flow, focusing on small scales. We confirm the existence of local isotropy of pair dispersion at scales smaller than a characteristic shear length scale $L_\Gamma = (\epsilon/\Gamma^3)^{1/2}$, where ϵ and Γ are the mean dissipation rate and shear rate, respectively. Furthermore, we show that pair dispersion in this locally isotropic regime is a scale-dependent super-diffusive process, similar to what occurs in homogeneous isotropic turbulent flows. In addition, we measure the pair relative velocity correlation function, showing that its de-correlation occurs in the locally isotropic regime, and discuss the implications of this observation for modelling pair dispersion. Thus, our study extends the fundamental understanding of turbulent pair dispersion to the anisotropic inhomogeneous turbulent canopy flow, bringing valuable information for modelling scalar dispersion in the atmospheric surface layer.

Key words: dispersion, turbulent mixing

† Email address for correspondence: ronshnapp@gmail.com

1. Introduction

Transport, dispersion and mixing are essential processes that determine a myriad of physical phenomena with crucial importance to the environment. These processes are driven by the random advection induced by turbulent flows. In particular, numerous such processes occur in the so-called canopy flows, namely in the lower part of the atmospheric surface layer. Examples include the dispersion of viral particles and fungal spores, the ventilation of urban air pollution and the facilitation of vegetation transpiration by inducing humidity, CO_2 and heat fluxes. Our focus in this study is on pair dispersion in turbulent canopy flows, which involves studying the relative motion between Lagrangian fluid particles. As was shown by Batchelor (1952), the statistics of pair dispersion can be used to determine the variance of concentration fluctuations of advected passive scalars.

The study of canopy flows has garnered significant research attention over the past five decades, leading to a plethora of insightful discoveries. This field has witnessed substantial efforts, as evidenced by numerous comprehensive reviews that have effectively summarized the key findings (Raupach & Thom 1981; Finnigan 2000; Britter & Hanna 2003; Belcher 2005; Brunet 2020). In neutrally stable conditions, canopy flows exhibit a distinctive feature characterized by the direct interaction between the fluid and large-scale wall-mounted obstacles within a boundary layer. This interaction generates a drag force that decelerates the flow within the canopy layer ($z < H$, where H represents the canopy height). At the upper boundary of the canopy ($z = H$), the drag discontinuity results in pronounced mean shear ($\partial U/\partial z$, where U is the mean streamwise velocity component and z is the vertical cordinate), giving rise to coherent Kelvin–Helmholtz structures akin to a mixing-layer analogy (Raupach, Finnigan & Brunet 1996). Turbulence statistics within the canopy layer are consequently both inhomogeneous and anisotropic. Eulerian single-point velocity probability density functions (PDFs) typically exhibit skewness, indicating intermittency and relatively high kurtosis values (Brunet, Finnigan & Raupach 1994). Interestingly, Lagrangian velocity increments have been observed to follow a Gaussian distribution (Shnapp *et al.* 2020). Additionally, turbulence in canopy flows is typically generated through two interdependent mechanisms: (I) shear production near $z \approx H$, and (II) production of smaller-scale turbulence within the wakes of the obstacles within the canopy ($z < H$) (Finnigan 2000).

A common framework for modelling dispersion in canopy flows is through Lagrangian stochastic models (DePaul & Sheih 1986; Raupach 1987; Baldocchi 1997; Katul *et al.* 1997; Reynolds 1998; Aylor & Flesch 2001; Poggi, Katul & Albertson 2006; Wilson *et al.* 2009; Duman *et al.* 2016; Bailey, Stoll & Pardyjak 2018; Fattal *et al.* 2021, 2023). In such models, Lagrangian fluid particles are advanced through the flow field using random walks that simulate the turbulent flow; this allows estimates of the statistics of the concentration field as a result of a certain distribution of scalar sources. Although these types of models allow us to bypass such difficulties as the hindering of parameterizations due to the existence of multiple scales or the inaccuracy of Taylor's frozen-turbulence hypothesis (Raupach & Thom 1981; Raupach 1987), there are still numerous open issues in their development and formulation. For the case of single particle motion, these issues include the non-uniqueness of first-order Markov random walk models in three dimensions (Thomson 1987), the effects of coherent structures (Raupach *et al.* 1996; Ghisalberti & Nepf 2002), non-Gaussian velocity PDFs (Pope & Chen 1990), the parallel contributions of wake and shear production (Shnapp *et al.* 2020) or the mechanical diffusion (Nepf 1999). To the best of our knowledge, previous studies have only considered the motion of single particles, and there are no previous studies that deal with the relative motion between particles in canopy flows. Notably, a full description of the dispersion of a group

of particles demands that the relative motion between any of their possible combinations be resolved (Batchelor 1952). Pair dispersion deals with the relative motion of pairs of particles, thus making a step forward in this respect.

In this work, we present an analysis of pair dispersion in a canopy flow using results from a wind tunnel experiment. This flow mimics the neutrally buoyant atmospheric surface layer in an environmental wind-tunnel set-up, as we reported in Shnapp *et al.* (2019). We focused in the past on single-particle statistics of this canopy flow, revealed short decorrelation Lagrangian time scales (Shnapp *et al.* 2020), and characterized the unique features of Lagrangian intermittency in this flow (Shnapp 2021). Our results deal with relatively small scales and are relevant for describing dispersion in between roughness elements inside the canopy. These findings are useful for instance for modelling dispersion between buildings in urban areas.

Background on pair dispersion and details on the experiment are given next. Following that, our analysis is divided into two main parts. First, we quantify the effect of the mean shear and anisotropy in our canopy model through the pair-dispersion tensor. Following that, we study the different regimes of pair dispersion that are observed in our measurement, including the ballistic and the inertial regime with a scale-dependent diffusivity; we suggest how these results could be useful for estimating the concentration variance of released passive scalars in the flow. Thus, our results could be useful for constructing and validating turbulent dispersion models in the atmospheric surface layer.

1.1. *Background on pair dispersion in isotropic and anisotropic turbulence*

Turbulent pair dispersion was introduced by Richardson (1926) and, since then, it has been studied extensively, e.g. as reviewed in Salazar & Collins (2009), Falkovich, Gawędzki & Vergassola (2001) and Sawford (2001). Pair dispersion describes the statistics of vector $\boldsymbol{r}$ connecting two, initially close, Lagrangian fluid particles

$$\boldsymbol{r} = \boldsymbol{x}^{(1)} - \boldsymbol{x}^{(2)}; \quad r \equiv |\boldsymbol{r}|, \tag{1.1}$$

where $\boldsymbol{x}^{(i)}$ is the three-dimensional (3-D) coordinate of a particle i (bold symbols denote vectors). Leaning on principles of homogeneous isotropic turbulence (HIT), the dynamics of r can be divided into three distinct regimes. (I) At short times, there is a ballistic regime (Batchelor 1952), during which particles' relative motion is co-linear. (II) At larger time scales, Richardson (1926) suggested that statistics of r can be modelled as a diffusive process with a scale-dependent diffusivity parameter, K

$$K \equiv \frac{1}{2}\frac{\partial\langle r^2\rangle}{\partial t} \quad \text{with } K \propto \langle r^2\rangle^{2/3} \sim r^{4/3}, \tag{1.2}$$

where $\langle\cdot\rangle$ is an ensemble average of many particle pairs. The scaling of K, commonly termed 'the four-thirds law', leads to a super-diffusive growth of the separation distance with $\langle r^2\rangle \sim \tau^3$ (Monin & Yaglom 1972). (III) At later times, when the two particles have separated farther away than the integral turbulence scale, i.e. for $r \gg L$, the distance r is expected to be diffusive with a constant, or Taylor, diffusivity (Taylor 1922)

$$K = T_L\tilde{u}^2, \tag{1.3}$$

where T_L is the Lagrangian time scale and $\tilde{u}$ is the root-mean-square (r.m.s.) of velocity fluctuations. Therefore, considering an ensemble of pairs of particles, initially separated by r_0 and moving in a HIT flow, the second-order moment of the distance, the variance

of the change in separation distance is summarized as follows (Salazar & Collins 2009; Monin & Yaglom 1972):

$$\langle (r - r_0)^2 \rangle = \begin{cases} \frac{11}{3} C_2 (\epsilon r_0)^{2/3} \tau^2 & \text{for } \tau \ll \tau_b \\ g \epsilon \tau^3 & \text{for } \tau_b \ll \tau \ll T_L \\ 2 \tilde{u} T_L \tau & \text{for } T_L \ll \tau \end{cases}, \tag{1.4}$$

where $C_2 \approx 2.1$ (Sreenivasan 1995) is the so-called Kolmogorov constant, ϵ is the mean rate of the turbulent kinetic energy dissipation, $g \approx 0.5$ (Ott & Mann 2000) is the so-called universal Richardson constant and the Batchelor time scale is defined as

$$\tau_b = \left(\frac{r_0^2}{\epsilon} \right)^{1/3}, \tag{1.5}$$

with τ the time elapsed since the pair began their separation, starting from r_0.

The theory of pair dispersion has been critically revised and extended in recent years. In particular, the three regimes have been tested in several experiments and numerical simulations for various initial distances, r_0/η (where $\eta = (\nu^3/\epsilon)^{1/4}$ is the Kolmogorov dissipation length scale). Verification tests of (1.4) in Yeung (1994), Ott & Mann (2000), Boffetta & Sokolov (2002*a*), Biferale *et al.* (2005), Berg *et al.* (2006), Bourgoin *et al.* (2006), Ouellette *et al.* (2006*b*), Elsinga, Ishihara & Hunt (2021) and Shnapp *et al.* (2023) have shown that it is difficult to observe the transition from ballistic to the super-diffusive regime, partly because it requires long-duration tracking, i.e. for $\tau \gg \tau_b$, and high Reynolds number flows (Berg *et al.* 2006; Bourgoin *et al.* 2006; Ouellette *et al.* 2006*a*). Specifically, the super-diffusive regime is asymptotic, and so finite Reynolds number effects cause the evolution of statistics of r to depend strongly on the initial separation, r_0/η (Biferale *et al.* 2005). Another issue is the strong intermittency of pair dispersion (Bitane, Homann & Bec 2012; Scatamacchia, Biferale & Toschi 2012; Biferale *et al.* 2014; Thalabard, Krstulovic & Bec 2014; Shnapp & Liberzon 2018), presumably due to Lagrangian statistics associated with long-time correlations (Boffetta & Sokolov 2002*b*). In particular, recent observations have shown that the scaling of $\langle r^2 \rangle$ depends on the initial conditions, namely on the initial separation (Elsinga *et al.* 2021; Tan & Ni 2022; Shnapp *et al.* 2023) and the initial separation velocity (Shnapp & Liberzon 2018), while it is also known that particles may retain their separation distance for very long times (Scatamacchia *et al.* 2012). Thus, it was suggested that Richardson's diffusive approach relies on an assumption of short Lagrangian correlation times (Bitane *et al.* 2012), which could explain the inconsistency with the recent observations. Several models using different forms of the so-called persistent ballistic random walks have been proposed as alternatives (Sokolov, Klafter & Blumen 2000; Rast & Pinton 2011; Thalabard *et al.* 2014; Bourgoin 2015). Bitane *et al.* (2012) proposed an alternative to τ_b which renders the process self-similar with respect to r_0; this framework is discussed in more detail below.

While (1.4) and the studies mentioned above pertain to HIT flows, pair dispersion in inhomogeneous or anisotropic flows has received much less attention. In inhomogeneous and anisotropic flows, statistics vary for each component of $\boldsymbol{r}$, and their evolution may be co-dependent on each other. In particular, in anisotropic flows, it is necessary to introduce a pair-dispersion tensor with components (Batchelor 1952)

$$\Delta_{ij}(\tau) = \langle (r_i - r_{i,0}) \cdot (r_j - r_{j,0}) \rangle; \tag{1.6}$$

notably, $\mathrm{tr}(\Delta_{ij}) = \langle (r - r_0)^2 \rangle$, and in HIT Δ_{ij} is diagonal. Furthermore, pair dispersion in anisotropic flows can depend on the initial orientation of $\boldsymbol{r}_0$ with respect to the

production mechanisms of turbulent kinetic energy; for shear flows, such as the canopy flow considered here, this would be the mean shear direction.

Shear effects on pair dispersion were studied previously in homogeneous shear flows through computational simulations. Shen & Yeung (1997) established that the presence of a mean shear has a strong effect on pair dispersion: it makes the evolution of Δ_{ij} anisotropic and with non-zero non-diagonal components, and it can render apparent super-diffusivity at long times ($\Delta_{xx} \sim \tau^3$) irrespective of the argument of scale dependence. More recently, Pitton *et al.* (2012) and Polanco *et al.* (2018) studied pair dispersion in turbulent channel flows and highlighted the combined effects of both anisotropy and inhomogeneity with respect to the distance from the wall. Their analysis clearly showed that where the mean shear is strongest the anisotropy of pair dispersion is most dominant. In a direct numerical simulation of a square duct flow, Sharma & Phares (2006) reported that particles remained trapped in secondary flow regions which affected the power law behaviour of $r(\tau)$. Celani *et al.* (2005) have proposed that mean shear and turbulent fluctuations act on pair dispersion on different time scales, which leads to two distinct regimes of either turbulent fluctuation dominance or mean shear dominance. A cross-over between these two regimes was predicted to occur at a critical time scale that is proportional to the mean shear $\tau_c \sim (\mathrm{d}U/\mathrm{d}z)^{-1}$. Recent studies further examined buoyancy-driven flows (Schumacher 2008; Ni & Xia 2013; Liot *et al.* 2019) and pair dispersion of inertial particles (Pitton *et al.* 2012) or in other complex flows, such as in the stroke of a swimming jellyfish (Kim & Chamorro 2019).

Despite the extensive body of work, the above discussion establishes the existence of a wide gap in the understanding of turbulent pair dispersion. Indeed, even for ideal cases, such as HIT or homogeneously sheared turbulence, our understanding is lacking and the introduction of flow inhomogeneity brings on another dimension of complexity. In this study, we bring the first empirical results on pair dispersion from an inhomogeneous and anisotropic canopy flow in order to shed some light on the prevailing issues.

2. Methods

2.1. *A 3-D particle tracking wind-tunnel experiment*

We study pair dispersion in a canopy flow using the results of a 3-D particle tracking velocimetry experiment (3D-PTV Malik, Dracos & Papantoniou 1993; Mass, Gruen & Papantoniou 1993; Dracos 1996). In the experiment, we obtained flow tracer trajectories in a wind-tunnel canopy flow model using an extended, real-time image processing system (Shnapp *et al.* 2019). The wind-tunnel laboratory, situated at the Israel Institute for Biological Research (Ness Ziona, Israel), features a 14 metre long, open circuit suction wind tunnel with a 2×2 squared metre cross-sectional area, that is fit for conducting experiments that mimic turbulent flows in the atmospheric surface layer (Bohbot-Raviv *et al.* 2017). The canopy flow was modelled by placing flat rectangular plates along the entire bottom wall of the test section (figure 1*d*). Our study used an inhomogeneous canopy layer, constructed with two types of flat plates with heights either H or $\frac{1}{2}H$, and width $\frac{1}{2}H$, where $H = 100$ mm; the two types of plates were positioned in consecutive rows and at a staggered construction, see figure 1. The canopy frontal area density, defined as $\Lambda_f = A_f/A_T$, (A_f being the element frontal area, and A_T the lot area of the canopy) is $\frac{1}{2}$, which positions our canopy between the 'dense' and 'sparse' categories (Brunet 2020). Data were gathered at two levels of the free-stream velocity, $U_\infty = 2.5$ and 4 m s^{-1}, being the free-stream mean velocity measured with a sonic anemometer at

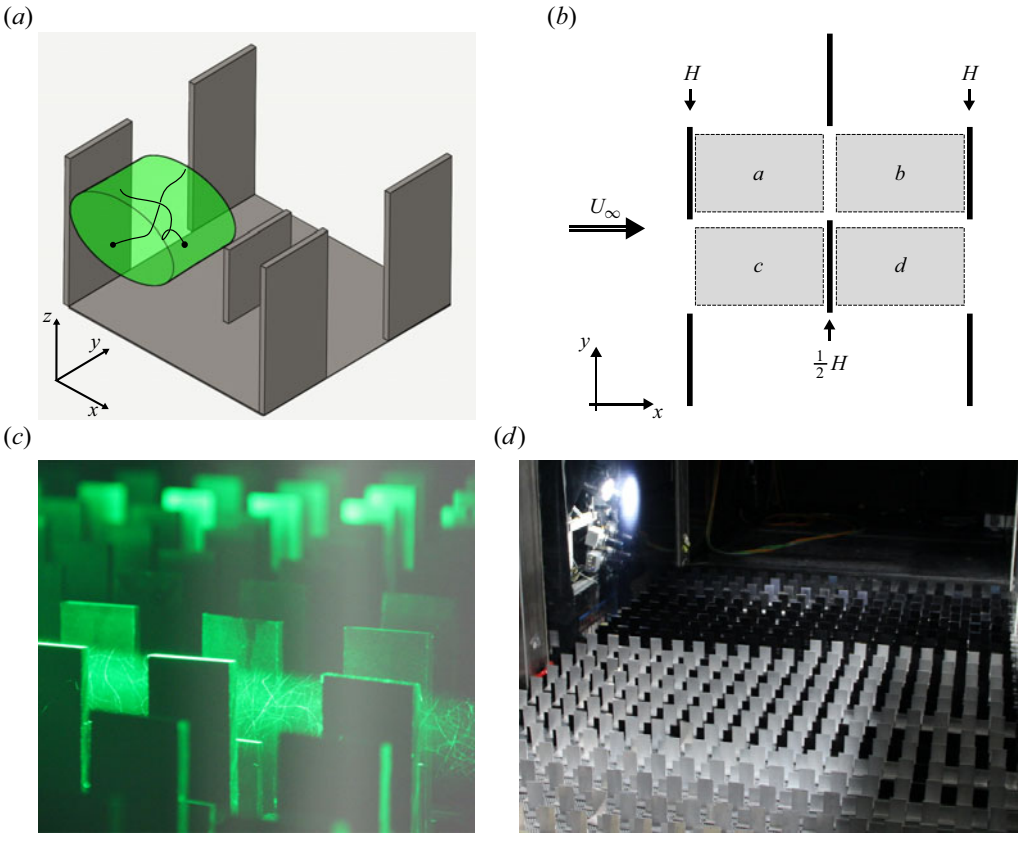

Figure 1. The canopy layer model used in the experiment. (*a*) An isometric view schematic sketch of the coordinate system, several roughness elements and a cutout laser beam illuminating a single sub-volume with tracer particles. (*b*) A top view schematic sketch of the measurement volume showing the 4 horizontal sub-volume positions. (*c*) An image of the canopy roughness elements with the laser beam and seeding particles seen passing through it. (*d*) A part of the wind-tunnel test section with the roughness elements placed on the bottom wall; the four camera system is seen outside of the test section, directed at the measurement region.

the centre of the wind-tunnel cross-section. These values correspond to Reynolds numbers $Re_\infty \equiv U_\infty H/\nu \approx 16 \times 10^3$ and 26×10^3, where ν is the kinematic viscosity of the air.

In the experiment, we tracked the positions of flow tracers using the 3D-PTV method through an extended 3D-PTV application. The details of the methods are given in Shnapp *et al.* (2019), so only brief information shall be repeated here for completeness. The flow was seeded with hollow glass spheres with an estimated Stokes number of $\overline{St} \approx 0.05$, indicating good tracking properties with only a minor filtration of high-frequency contents of the turbulent dynamics that cannot be ruled out. The particles were added to the air flow inside the test section, far upstream of the measurement region through four nuzzles connected to a fluidized bed reactor. The particles were then carried by the air flow in the wind tunnel down to the measurement region, where they were illuminated with a 10 W continuous wave laser beam, as shown in figure 1(*a*) and 1(*c*). A set of four 4-megapixel cameras captured images of the tracer particles at a rate of either 500 or 1000 Hz, depending on the height at which data were gathered. The images from each camera were fed into a dedicated FPGA card for online image analysis and particle segmentation on the hardware, and the particle two-dimensional (2-D) positions were saved for post-processing

in a compact binary format. This recording system, internally called 'Blob Recorded', allows unprecedentedly long 3D-PTV experimental campaigns to be performed due to the achievable $O(10^4)$ data compression ratio, see Shnapp *et al.* (2019). Following that, we used the open source software OpenPTV (OpenPTV Consortium 2004) to perform camera calibration, stereo matching and tracking. Finally, particle positions were smoothed and the velocities and accelerations were calculated by local spline fitting following the method introduce in Luthi, Tsinober & Kinzelbach (2005). To ensure good trackability of the particles in the high-speed wind-tunnel air flow we used rather low seeding values of the order of 20 particles per image; together with very long recording durations, approximately 15 minutes long in each location, we ensured that the statistics we gathered represent the flow well. The imaging resolution we used was 50 μm per pixel, and the region of measurement was divided into sub-volumes, approximately $8 \times 5 \times 4$ mm^3 in size (full description is given in § 2.3). The data analysis was performed using the open source Flowtracks package (Meller & Liberzon 2016). In this work, we use the frame of reference that is commonly used in the canopy flow literature: x is aligned with the streamwise direction longitudinally within the wind tunnel, y is the cross-stream horizontal direction and z points vertically up against gravity and away from the bottom wall.

2.2. *The canopy flow model*

The canopy model in the experiment had a flow structure with characteristics that resemble those typically observed in neutrally buoyant canopies (Finnigan 2000), however, with certain unique features that were the result of the double-height construction we used. The double-averaged mean velocity profile demonstrates an inflection point slightly above the roughness elements. Our previous work with this canopy construction, based on particle image velocimetry measurements, showed a smaller shear length at the top of the canopy as compared with homogeneous canopy layers at similar densities and that, unlike homogeneous canopies, it had a second inflection point right above the lower roughness elements (Shig *et al.* 2023*a*). The velocity component distributions were anisotropic, they become broader with z, and a pronounced positive skewness was present in the distributions of the streamwise velocity component (Shnapp *et al.* 2019); this skewness is a hallmark of the sweep events that characterize the roughness layer ($z < 1.5H$) in canopy flows (Brunet *et al.* 1994; Raupach *et al.* 1996). In addition to that, a second peak of increased sweep contribution above the lower set of elements appeared due to the double-height canopy construction (Shig *et al.* 2023*b*).

From the Lagrangian statistics point of view, our previous analysis of 3D-PTV measurements showed that the canopy is characterized by an unexpectedly short Lagrangian de-correlation time scale (Shnapp *et al.* 2020). This feature leads to PDFs of velocity increments that are of a Gaussian shape despite the marked non-Gaussianity of the absolute velocity components. In addition to that, single-particle velocity statistics were found to exhibit both the characteristic small-scale Lagrangian intermittency (Arnèodo *et al.* 2008), and a so-called large-scale intermittency due to the sweep–ejection cycle of the canopy flow (Shnapp 2021).

2.3. *Data analysis: a quasi-homogeneous approach*

We recorded trajectories in the height range $0.5H < z < 1.5H$ and across a single representative canopy unit cell, by scanning the full volume through 20 sub-volumes, as depicted by the green shaded region in figure 1(*a*). The sub-volumes were defined at 4 horizontal locations, and at 5 different heights above the wind-tunnel bottom wall.

Sub-volume horizontal positions are labelled alphabetically a, b, c and d, as shown in figure 1(b). At each position, a–d, we used 5 vertical slabs of thickness $0.2H$ to define the sub-volumes; the vertical slab positions are labelled numerically 1–5 and correspond to heights $z/H \in \{0.5\text{–}0.7, 0.7\text{–}0.9, 0.9\text{–}1.1, 1.1\text{–}1.3, 1.3\text{–}1.5\}$, respectively. The volume scanning approach allowed us to measure a full canopy unit cell, however, it limited the particle trajectory lengths to be within each of the individual sub-volumes.

In the frame of our analysis, we present statistical properties calculated over ensembles of trajectories. Thus, formally, the mean value of any Lagrangian quantity A is estimated using the average

$$\langle A \rangle \equiv \frac{1}{N} \sum_{i=0}^{N} A_i(\boldsymbol{x}_{\mathbb{V}}, t), \tag{2.1}$$

where $\mathbb{V}$ is a tag pertaining to different particle ensembles. In our recent work (Shnapp *et al.* 2020), we explored single-particle statistics using the same dataset. There, the sub-volume-averaged quantity approach was proposed, in which Lagrangian statistics were presented for ensembles of particles found at each sub-volume, essentially resulting in spatially averaged statistics across each small sub-volume. It was furthermore shown that this quasi-homogeneous approach is justified in our flow because the random turbulent forcing outweighed the combined effects of flow inhomogeneity terms in the stochastic particle equation of motion. Specifically, this was achieved through the condition

$$\left\langle \frac{1}{2} \frac{|C_0 \epsilon R_{ij}^{-1} u_j'|}{|\phi_i/g|} \right\rangle \ll 1, \tag{2.2}$$

where C_0 is the so-called Lagrangian structure function coefficient, $R_{ij} = \langle u_i' u_j' \rangle$ is the Reynolds stress tensor, u_j' is the r.m.s. of the j velocity component and ϕ_i/g is a vector representing a sum of drift terms of the Lagrangian velocity PDF that allows us to account for flow inhomogeneity (Thomson 1987). In the present work, we capitalize on the condition (2.2), and present quasi-homogeneous statistics for pair dispersion as well. This point is important since it validates the effective scaling laws we obtain below.

In addition to that, in Shnapp *et al.* (2020), turbulent parameters of our flow were calculated where they were discussed and analysed in depth. In particular, we calculated ϵ, the turbulence dissipation length and time scales η, τ_η, the Lagrangian decorrelation time scale T_i and the Taylor Reynolds number Re_λ. The values of these parameters are tabulated for each sub-volume in the Appendix, and they shall be used in the analysis below.

3. Local isotropy of pair dispersion

3.1. *Scaling analysis*

As discussed in § 1, numerical simulations (Shen & Yeung 1997; Sharma & Phares 2006; Pitton *et al.* 2012; Polanco *et al.* 2018; Polanco 2019) confirmed theoretical predictions (Monin & Yaglom 1972) that the mean shear, inhomogeneity and/or anisotropy in the flow cause anisotropic pair dispersion. This is based on the fact that the fundamental mechanism driving pair separation is the relative velocity between Lagrangian particles. Because turbulent flow statistics are scale dependent, it is expected that also the 'degree' of anisotropy in pair dispersion will depend on the separation distance r. Empirical evidence shows that turbulent velocity fluctuations are characterized by a tendency to recover isotropy at small scales, a phenomenon dubbed the return to isotropy (Lumley & Newman

1977). The return to isotropy at smaller scales was also observed in canopy flows (Stiperski, Katul & Calaf 2021). This suggests that, at sufficiently small values of r, and as long as the Reynolds number is sufficiently high, pair dispersion will be at least approximately, isotropic, as predicted theoretically in Celani *et al.* (2005). Thus, to determine whether local isotropy or anisotropy is expected to occur in our pair-dispersion measurement, we first conduct an analysis of the relevant scales of the flow.

Anisotropic turbulent fluctuations are introduced to the flow by the boundary conditions. In the canopy flow case, the flow impinges on the roughness obstacles that exert drag and retard the flow. Thus, the production of turbulence in canopies is commonly decomposed into two main contributions (Finnigan 2000): (I) shear production at the top of the canopy layer, and (II) production at smaller scales in the wakes of the obstacles. The third possible component, the production by wall friction, is usually negligible compared with form drag due to the low velocity near the ground for sufficiently dense canopies. Because shear production occurs due to the interaction of the double-averaged mean shear and the Reynolds stress, it induces an intrinsic anisotropy in the structure of turbulence in canopy flow. On the other hand, wake production occurs due to local variations in the rates of strain, associated with the wakes and boundary layers of individual roughness elements (Finnigan 2000). Since the local orientation of most straining directions changes in space, we expect that the anisotropy in the pair-dispersion statistics will mostly reflect shear production, at least to a first approximation. This seems to be particularly true for Lagrangian statistics such as in pair dispersion since the particles essentially sample different flow regions.

The appropriate length scale that characterizes the production of turbulence by shear is

$$L_\Gamma = \left(\frac{\epsilon}{\Gamma^3}\right)^{1/2}, \tag{3.1}$$

where $\Gamma = \mathrm{d}U/\mathrm{d}z$ is the mean velocity gradient. Indeed, analysing the scale-by-scale turbulent kinetic energy budget in turbulent shear flows, Casciola *et al.* (2003) showed that the production by shear continues down to L_Γ, whereas for scales $r < L_\Gamma$ the turbulent kinetic energy transport becomes more dominant. For our analysis, we parameterize the shear length using a global, canopy-wide, measure of the mean velocity gradient $-\Gamma_z = U(z = 1.5H)/1.5H \approx 4.75\ \mathrm{s}^{-1}$. Figure 2(*a*) shows that L_Γ/η increased from roughly 100 inside the canopy and up to roughly 150 above it.

Another critical dimension of pair dispersion is time. Celani *et al.* (2005) predicted that, for particles with sufficiently small initial separations, pair dispersion is initially isotropic while it becomes anisotropic once the particles have grown sufficiently far apart for the anisotropic turbulent scales to be prominent. They further noted that the critical time scale for this transition is proportional to the inverse mean shear rate, $\tau_c \sim \Gamma^{-1}$. Figure 2(*b*) shows the Lagrangian velocity decorrelation time scale for the streamwise velocity component normalized by Γ. Throughout our measurement region, we observe that $T_x{\cdot}\Gamma < 1$.

Due to the finite measurement region, our work focuses on time scales up to $\tau \approx T_x$. In addition, the typical separations between particles that we consider in our work reach up to roughly $r = 100\eta$, namely, mostly values with $r < L_\Gamma$. Thus, the dimensions of our measurement region and the time scales on which we focus are smaller than the scales imposed by the mean shear. For this reason, we expect to see only weak anisotropy in pair-dispersion statistics due to the local isotropy of the flow.

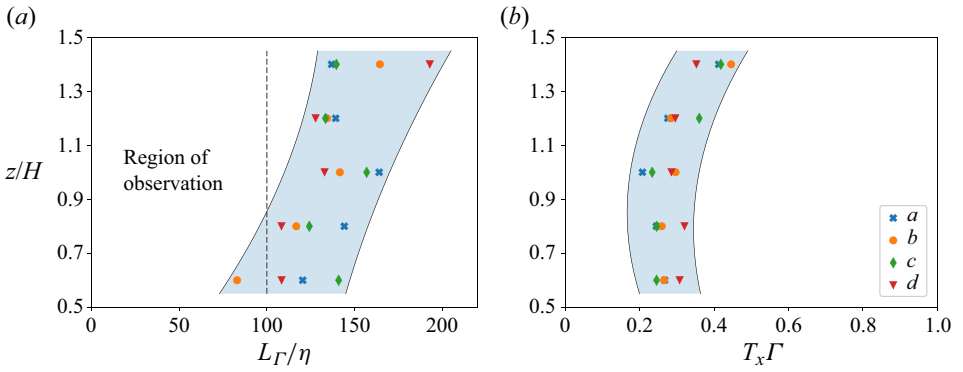

Figure 2. (*a*) Ratio of the shear length scale and the Kolmogorov length scale for the various sub-volumes plotted as a function of height. (*b*) The Lagrangian velocity decorrelation time scale, T_x, normalized using the mean shear rate plotted as a function of height. Data are shown for the $Re_\infty = 26 \times 10^3$ case.

3.2. *Observation of weak anisotropy*

The various components of the pair-dispersion tensor, Δ_{ij}, across the whole region of measurements are shown in figure 3 for two representative initial separation values inside the inertial range. In all cases, the diagonal components steadily increase from zero as time increases, which indicates increasing separations in all orthogonal directions, as expected. The off-diagonal components, on the other hand, generally do not increase significantly in the available time frame of the measurements, with a trend for larger scatter for the larger initial separation cases and at longer times. This occurs consistently across the entire measurement sub-volumes.

Since the non-diagonal components represent mixed averages of the separation vector's components, their relatively low values indicate a weak correlation among the separations in different directions. This behaviour is unlike what is expected in a mean shear-driven separation scenario as, for example, in homogeneously sheared turbulence the separation velocity in the streamwise direction grows as the separation along the mean velocity gradient direction increases. Thus, the behaviour observed for Δ_{ij} is consistent with the notion presented in § 3.1 that the mean shear is not expected to significantly affect pair dispersion in our measurements.

The three diagonal components of the pair-dispersion tensor grow with time, and slightly different values are seen for the various components. To highlight these differences we introduce the following tensor:

$$I_{ij} \equiv \frac{\Delta_{ij}}{\mathrm{tr}(\Delta_{ij})} - \frac{1}{3}\delta_{ij}, \tag{3.2}$$

where δ_{ij} is the identity matrix. The tensor I_{ij} shows the statistics of the components of $\boldsymbol{\Delta r}$ with respect to their norms, essentially highlighting anisotropy. Let us note that $\mathrm{tr}(I_{ij}) = \sum_i I_{ii} = 0$, and that dispersion in the direction of components with $I_{ii} > 0$ is faster than in the isotropic case (i.e. than $\frac{1}{3}\langle (r - r_0)^2 \rangle$), while for components with $I_{ii} < 0$ the dispersion is slower. In a limiting case in which pairs separate only in one direction, say x, then $I_{xx} = \frac{2}{3}$ while $I_{yy} = I_{zz} = -\frac{1}{3}$.

Histograms of the diagonal components, $I_{ii}(\tau)$ are shown in figure 4, focusing on two representative initial separations and three representative heights: inside the canopy $0.5 < z/H < 0.7$, at its top $0.9 < z/H < 1.1$ and above it $1.3 < z/H < 1.5$. The histograms

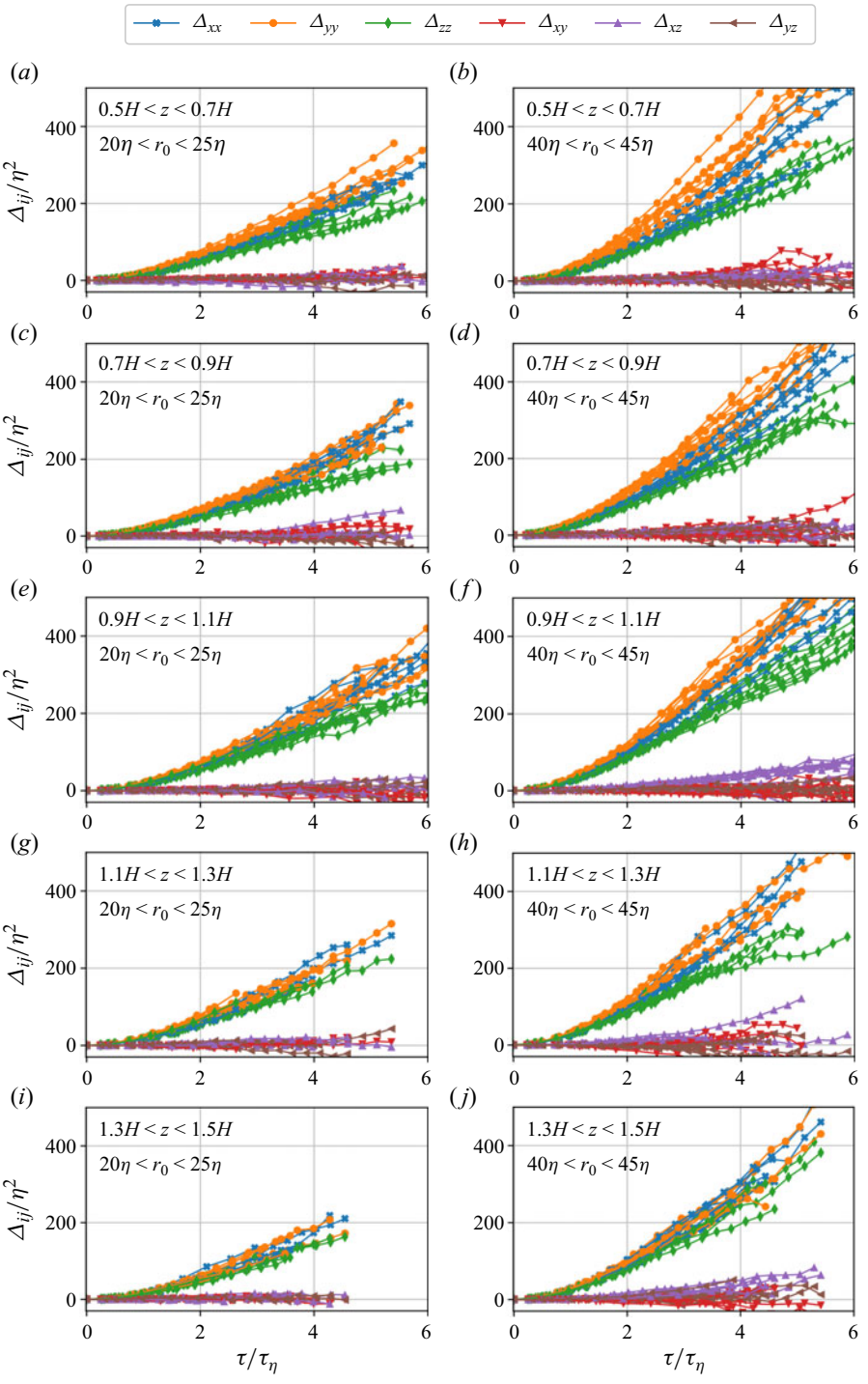

Figure 3. The various components of the pair-dispersion tensor are shown for two initial separation values and at the five height groups used. Different shapes correspond to different components of Δ_{ij}. Lines with the same shape come from each of the four horizontal sub-volume locations and thus represent the horizontal variability of the statistics.

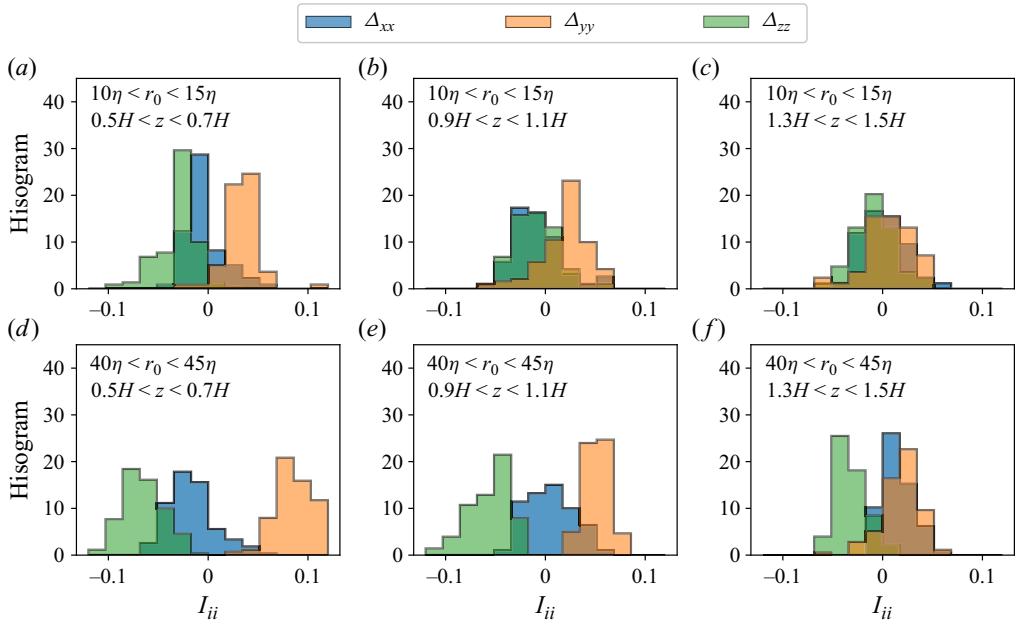

Figure 4. Diagonal terms of the pair-dispersion tensor normalized by its trace minus one third. Data are shown for sub-volumes at three heights and for two levels of r_0.

count data points from all horizontal positions, both Re_∞, and across the time range $\tau < 6\tau_\eta$, during which I_{ii} did not change appreciably.

The disparity between the separation components decreases with height, being the largest inside the canopy and smallest above it. Furthermore, the increase in separation was the slowest in the vertical direction and the fastest in the spanwise direction, whereas the increase of the streamwise separation was approximately at isotropic values ($I_{xx} \approx 0$). The fact that the separation is fastest in the spanwise direction and inside the canopy suggests that the observed anisotropy could be attributed to the channelling of the flow in between the roughness obstacles, which were in a staggered configuration, and not necessarily due to the effects of the mean vertical shear. This would highlight the effects of dispersive fluxes between the canopy obstacles in driving horizontal dispersion. And still, we note that the magnitudes of I_{ii} values reach only up to approximately 0.1; this corresponds to a weak anisotropy with 20 % of disparity between the separation in the vertical and spanwise components. In particular, this degree of anisotropy is much smaller than what was observed in previous works concerning flows with mean shear (Shen & Yeung 1997; Pitton *et al.* 2012; Polanco *et al.* 2018).

The disparity between the components is also seen to increase with the initial separation, r_0. This is consistent with the picture of return to isotropy, as anisotropy becomes more prominent at larger scales (Lumley & Newman 1977).

The increase of anisotropy with scale brings up questions regarding the development of anisotropy in pair dispersion with time. As particles separate, the growth of typical r values suggests that pairs are exposed to the more anisotropic turbulent scales as time increases. The development of anisotropy could be examined by adopting a framework analogous to the one introduced by Stiperski *et al.* (2021), which used a projection of the invariants of the normalized Reynolds stress tensor on a 2-D plane, allowing them to investigate trajectories of the return to isotropy in various canopy flows. In an analogy to

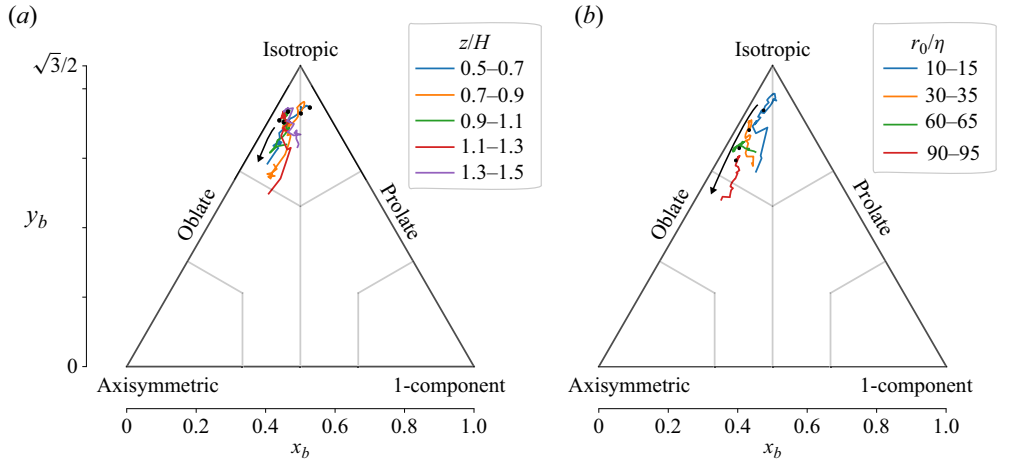

Figure 5. Trajectories of pair-dispersion anisotropy on the x_b–y_b plane. Two datasets are shown: for five heights with $15\eta r_0 < 20\eta$ (*a*) and for four initial separation values with $0.9H < z < 1.1H$ (*b*). The beginning of each trajectory, i.e. at time zero, is marked by a black circle, from which the trajectories evolve with time up to $7\tau_\eta$. Data are for the $Re_\infty = 2.6 \times 10^4$ case, and horizontally averaged across all sub-volumes.

that, we examine here the projection of the eigenvalues of I_{ij} using the same projection

$$\left.\begin{aligned} x_b &= \lambda_1 - \lambda_2 + \frac{1}{2}(3\lambda_3 + 1) \\ y_b &= \frac{\sqrt{3}}{2}(3\lambda_3 + 1) \end{aligned}\right\}, \tag{3.3}$$

where λ_1, λ_2 and λ_3 are the smallest, intermediate and largest eigenvalues of I_{ij}, respectively. Equation (3.3) maps the eigenvalues to a planar equilateral triangle. As seen in figure 5, the triangle's nodes correspond to cases of fully isotropic, 2-component axisymmetric or one-component dispersion. Plotting the trajectories that correspond to the measured I_{ij} tensor allows us to probe the topology of pair dispersion as it varies in time. For almost all of the data shown, the weak anisotropy of pair dispersion is seen by the fact that the trajectories are almost completely confined to the isotropic part of the map. Nevertheless, the weak anisotropy that does exist is evident in the general trend of trajectories to progress along the left flank of the triangular maps, in the direction corresponding to the oblate topology. The trajectories also demonstrate that most of the anisotropy in our pair-dispersion measurements is explained by the larger initial separation values and not due to the increase in separation with time. This is in line with the fact that our measurements are confined to time scales smaller than Γ^{-1}.

3.3. *Bias due to initial orientation*

As shown in Shen & Yeung (1997), Pitton *et al.* (2012) and Polanco *et al.* (2018), in flows with mean shear, pair dispersion is affected by the initial orientation of the pairs for short times. Indeed, taking as an example the case of a shear flow where the velocity is $\boldsymbol{u} = (\Gamma z, 0, 0)$ and considering particles with an initial separation $\boldsymbol{r}_0 = (r_{0,x}, r_{0,y}, r_{0,z})$, then the separation vector is $\boldsymbol{r}(\tau) = (r_{0,x} + \tau\Gamma r_{0,z}, r_{0,y}, r_{0,z})$. Therefore, even in the simplest scenario, the presence of mean shear biases the streamwise separation component. The bias depends on the projection of the initial separation vector on the mean shear direction,

so for pairs whose $\boldsymbol{r}_o$ is aligned with the mean shear direction, the bias is by a factor of Γr_0.

The relative importance of this bias in a turbulent flow can be estimated by comparing Γr_0 with the spatial fluctuating velocity increments $\delta_{r_0} u$. If we apply the Kolmogorov dimensional scaling (Kolmogorov 1941) to parameterize $\delta_{r_0} u \sim (\epsilon r_0)^{1/3}$, we can construct a dimensionless group $S = \Gamma r_0/\delta_{r_0} u = \Gamma r_0^{2/3}/\epsilon^{1/3} = (r_0/L_\Gamma)^{2/3}$ that quantifies the importance of the shear bias for particles with r in the inertial range. When $S \gg 1$ we expect that shear will bias pair separation based on their initial orientation whereas when $S \ll 1$ it will not. Also, if an inertial range exists, this bias grows stronger as $r_0^{2/3}$ for smaller initial separations, which is in qualitative agreement with the observations of Shen & Yeung (1997) and Polanco *et al.* (2018). Also, in the dissipation range, the velocity field is presumably smooth and the typical size of velocity gradients is $1/\tau_\eta = (\epsilon/\nu)^{1/2}$ (where τ_η is the dissipation time scale). Therefore, the dissipation scaling for velocity increments in the dissipation range is $\delta_{r_0} u \sim r_0(\epsilon/\nu)^{1/2}$ so that the dimensionless parameter becomes $S = \Gamma(\epsilon/\nu)^{-1/2}$. To summarize, we define

$$S = \begin{cases} \Gamma \left(\dfrac{\epsilon}{\nu}\right)^{-1/2} & \text{if } r_0 \ll \eta \\ \left(\dfrac{r_0}{L_\Gamma}\right)^{2/3} & \text{if } r_0 \gg \eta \end{cases}, \tag{3.4}$$

and when $S \gg 1$ the presence of mean shear is expected to bias pair dispersion, making it faster when the initial orientation of particles is aligned with the shear direction.

To examine the effect of initial orientation in the canopy flow, we estimated the variance $\langle \delta r^2 \rangle$ conditioned on the initial orientation of $\boldsymbol{r}_0$. We divided the pairs into sub-samples based on the condition that the angle between $\boldsymbol{r}_0$ and each of the coordinate axes was lower than 25°. In figure 6, probability distributions are shown for the conditional variance normalized by the variance of all the pairs. In this case, data were taken at all available times, all sub-volumes, and with $30\eta < r_0 < 50\eta$. The distributions show that pairs with initial separation aligned vertically (i.e. with $\hat{z}$) typically separated faster than the average, whereas pairs with initial separation aligned with the spanwise (i.e. $\hat{y}$) typically separated slower than the average. Considering the previous observation that separations are fastest in the spanwise direction (figure 4), the bias observed here for vertically oriented pairs may suggest that the channelling effect varies with height. This is also consistent with the observation of the strongest anisotropy inside the canopy layer.

From figure 2 it is seen that for the present case, we have a maximum value of $S \approx 0.38$, which suggests that the bias should be quite weak. This is validated in figure 6 since it shows that the magnitudes of the pair-dispersion bias encountered in our measurements reached up to 30 % and was typically around 15 %. These values are indeed rather low considering that previous studies (Pitton *et al.* 2012; Polanco *et al.* 2018) observed orders of magnitudes of difference between different groups of conditioned particles in regions of the flow with strong shear.

Overall, our empirical results agree well with the scaling argument presented above and are consistent with the theory of Celani *et al.* (2005). These results reveal the important role of L_Γ and Γ in determining the scales relevant for the development of pair-dispersion anisotropy in canopy flows. Indeed, anisotropy was weak at the scales relevant to our work, in addition to a weak bias due to the initial orientation of pairs. These key results highlight local isotropic turbulent fluctuations as the main driver of particle separations in the canopy flow at small scales.

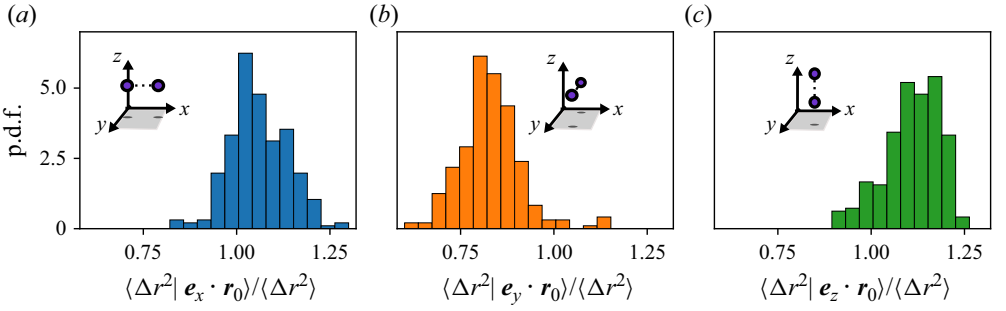

Figure 6. Probability distributions of the variance of change in separation distance conditioned on the initial orientation and divided by the unconditioned value. Data are taken at different times and all sub-volumes for pairs with $30\eta < r_0 < 50\eta$.

4. Regimes of pair dispersion and a scale-dependent diffusivity

Following the observation in § 3 that pair dispersion is only weakly anisotropic in our measurements, we focus next on statistics of the change of the separation distance, $r = |\boldsymbol{r}|$, with time. In particular, we analyse the scaling of the change in separation distance $\langle (r - r_0)^2 \rangle \propto \tau^\beta$ (Biferale *et al.* 2005; Berg *et al.* 2006; Ouellette *et al.* 2006*b*; Salazar & Collins 2009; Shnapp & Liberzon 2018). It is also noted that, formally, due to the inhomogeneity of our canopy flow, β is essentially an 'effective scaling'. Therefore, the goal of this section is to compare the empirical data with the different regimes of (1.4), in order to understand the phenomenology underlying pair dispersion in our canopy flow.

In order to investigate time scaling, it is essential to consider a possible bias due to the finite volume of measurement. In particle tracking experiments there is a concern that finite volumes could lead to a bias in the estimate of Lagrangian scaling exponents since particles leave the volume at different times. A similar bias when estimating Lagrangian correlation functions was investigated in Biferale *et al.* (2008). Specifically, the extreme cases in which particles separate very fast and leave the volume of measurement at short times could influence the slopes of the curves, leading to errors in estimating the scaling exponent β. To avoid such a bias, the data were sub-sampled for pairs tracked for a fixed amount of time. For our analysis, we consider only pairs that were successfully tracked for durations $t_{tr} > 5\tau_\eta$. Statistics were calculated only for $\tau \leq 5\tau_\eta$ (where t_{tr} is the tracking time, the duration of time for a particle to remain in the sub-volume). This sub-sampling may cause an underestimation of the rate of separation. However, it is necessary for making reliable estimations of the scaling exponent. In addition to that, to maintain a concise description we present data for only one sub-volume – b3, albeit the results were observed to be robust for particles from the other sub-volumes as well.

4.1. *The ballistic regime*

We first verify that pair dispersion at short times follows a ballistic propagation, as was suggested by Batchelor (1952). This regime is characterized by a quadratic growth of $\langle \Delta r^2 \rangle \propto \tau^2 (\tau \ll \tau_b)$, corresponding to the first case of (1.4). Figure 7(*a*) presents pair dispersion from the canopy flow in normalized form according to (1.4)

$$\frac{\langle \Delta r^2 \rangle}{S_{LL}(r_0)\tau_b} = \left(\frac{\tau}{\tau_b}\right)^2, \tag{4.1}$$

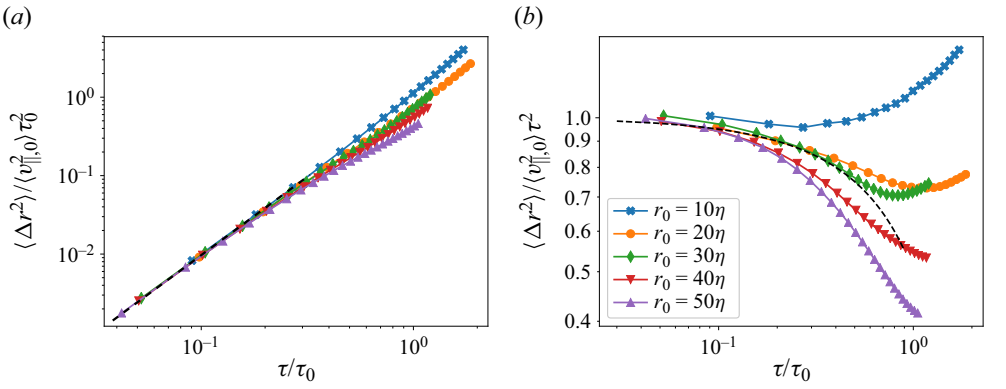

Figure 7. (*a*) Variance of the change in pair separation normalized with the second moment of separation velocities and the Batchelor time scale. The dashed line corresponds to the ballistic regime, (4.1). (*b*) Same data but normalized using the time lag, and the dashed line corresponds to (4.3).

where $S_{LL}(r_0) = \langle (\delta_{r_0} \boldsymbol{u} \cdot \boldsymbol{r_0}/r_0)^2 \rangle$ is the directly measured Eulerian structure function, and the Batchelor time scale τ_b. Initially, for $\tau < 0.1\tau_b$, all the curves with different initial separations collapse on a quadratic dashed line, as (1.4) suggests. Similar results were previously obtained in homogeneous flows by Ouellette *et al.* (2006*b*), Bitane *et al.* (2012) and Shnapp & Liberzon (2018), and inhomogeneous flows by Polanco *et al.* (2018), Liot *et al.* (2019) and Ni & Xia (2013). The collapse of the data at short times using the longitudinal structure function $S_{LL}(r_0)$ is important since it confirms that $[S_{LL}(r)]^{1/2}$ is the appropriate velocity scale for the separation of particles at a distance r.

4.2. *Transition from a ballistic to an inertial regime*

Next, we examine the termination of the ballistic regime, which is done following the analysis performed recently by Bitane *et al.* (2012) for the case of HIT flow. We denote the separation velocity $v_\parallel = \partial r/\partial t$ and acceleration $a_\parallel = \partial v_\parallel/\partial t$. Then, the separation distance is Taylor expanded to the third order, squared and ensemble averaged, which gives

$$\langle \Delta r^2 \rangle = \langle v_{\parallel,0}^2 \rangle \tau^2 + \tfrac{1}{2} \langle a_{\parallel,0}\, v_{\parallel,0} \rangle \tau^3 + O(\tau^4), \tag{4.2}$$

where subscript 0 denotes initial values at $\tau = 0$. This expression, which extends the Ballistic regime, is expected to hold for short times, and, in particular, according to Bitane *et al.* (2012), it gives the appropriate time scale for the end of the ballistic regime at $\tau_0 = -\langle v_{\parallel,0}^2 \rangle / \langle a_{\parallel,0}\, v_{\parallel,0} \rangle$. Note that the minus sign is used since in 3-D turbulence $\langle a_{\parallel,0}\, v_{\parallel,0} \rangle < 0$ (Ott & Mann 2000), as was confirmed for our data (not shown for brevity). Therefore, the above Taylor expansion can be rewritten in dimensionless form as

$$\frac{\langle \Delta r^2 \rangle}{\langle v_{\parallel,0}^2 \rangle \tau^2} = 1 - \frac{1}{2} \left(\frac{\tau}{\tau_0} \right) + O(\tau^2). \tag{4.3}$$

In figure 7(*b*) we show the empirical data of $\langle \Delta r^2 \rangle$ for the different r_0 cases, normalized according to the left-hand side of (4.3), and compare with the right-hand side shown as a dashed black line. For short times, $\tau \ll \tau_0$, the figure shows rather good agreement between the empirical data and (4.3), especially in the downward trend of the lines, which means that the above arguments of Bitane *et al.* (2012) agree with our data. Furthermore,

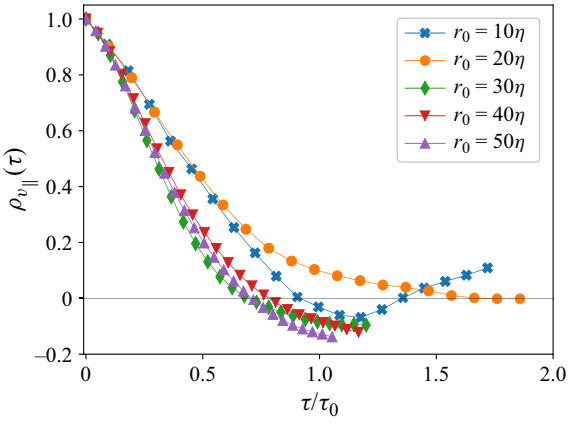

Figure 8. Autocorrelation functions of the rate of separation $v_\parallel$, shown against time normalized with τ_0.

the negative term in (4.3) is responsible for the deviations from a purely quadratic growth as time progresses. Therefore, defining the end of the ballistic regime as a deviation of $\langle \Delta r^2 \rangle$ by, say, 10 % from $\langle v_{\parallel,0} \rangle \tau^2$, we obtain that the ballistic regime ends at $\tau = 0.2\tau_0$. Indeed, our data from different r_0 agree with (4.3) (dashed line) roughly up to $\tau \approx 0.2\tau_0$. At longer times, $\tau \gtrsim 0.2\tau_0$, the normalized pair dispersion curves in figure 7(*b*) begin deviating upwards. The increase in of the curves slope signals an increase in the time scaling of the separation, which can be attributed to the end of the ballistic regime and a transition towards the inertial regime (transition from the first to the second case in (1.4)).

Once the ballistic regime is terminated, the separation velocities of particles have deviated significantly from their initial values. This can be shown by examining the autocorrelation of the separation velocity, defined here as

$$\rho_{v_\parallel}(\tau) = \frac{\langle v_\parallel(\tau) v_\parallel(0) \rangle}{\sqrt{\langle v_\parallel^2(0) \rangle \langle v_\parallel^2(\tau) \rangle}}, \tag{4.4}$$

which is shown in figure 8. The autocorrelation $\rho_{v_\parallel}$ is plotted against τ/τ_0 for the 5 cases of pairs with different r_0. The graph shows that the correlation of the separation velocity drops to roughly zero once the time lag is $\tau \sim \tau_0$ (with some weak dependence on r_0). This confirms that, at $\tau \gtrsim \tau_0$, the particles' separation was with velocities that are very different from their initial value. We shall call this regime of the pair-dispersion inertial regime.

4.3. *Scale-dependent growth rates and approach to Richardson's 4/3 law*

Richardson's classical theory (Richardson 1926) describes pair dispersion as an accelerating process in which the rate of separation increases with r. Accordingly, as r increases with time, we should observe that the separation rate grows as well. Nevertheless, as discussed in the introduction, this is often challenging to observe in experiments and simulations due to the need for sufficiently long observation times such that r increases significantly. To confirm whether such conditions occurred in our experiment we show in figure 9 the normalized separation, r/r_0, for five groups of pairs with different initial separations. For the group with the smallest initial separation available, $r_0 = 10\eta$, the typical separation increased by a factor of two by the end of our measurement range; on the other hand, the increase in separation was much lower for the other groups with

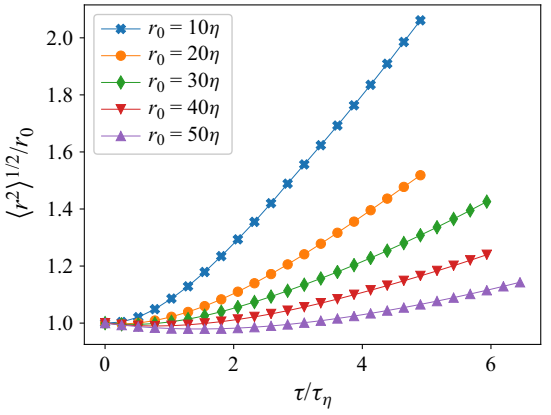

Figure 9. Root mean squared separation distance between trajectories, normalized with the initial separation and plotted against time lag normalized with the Kolmogorov time scale.

larger r_0. This issue, however, is typical in experiments and simulations (Ott & Mann 2000; Biferale *et al.* 2005; Liot *et al.* 2019; Elsinga *et al.* 2021; Tan & Ni 2022), because the separation time scale, $\tau_0 \sim r_0^{2/3}$, is smaller for smaller r_0. For this reason, if an explosive pair-dispersion regime occurred in our experiment, it should be most evident in statistics of particles with small initial separations. Indeed, in figure 7(*a*), an increase of the local slope for the $r_0 = 10\eta$ group can be seen at longer times ($\tau \geq \tau_0$), indicating an increase in local scaling exponent. In these cases, the pair dispersion is super-diffusive, i.e. $\langle \Delta r^2 \rangle \propto \tau^\beta$ with $\beta > 2$.

With the observations obtained thus far, let us lay out the reasoning to explain the behaviour of pair dispersion in figure 7 at longer times, namely after the Ballistic regime is over. First, for all cases of r_0 the separation velocity became decorrelated in our measurement (i.e. figure 8), so that a so-called inertial regime was reached. Notably, even for the largest initial separation considered, $r_0 = 50\eta$, we have still have $\tau_0/T_L \approx 0.96$, so the pairs did not enter yet into the asymptotic diffusive regime (third case in (1.4)). Second, the increase of r relative to its initial value depended on r_0, as shown in figure 9. Third, in Richardson's theory pair dispersion is described as a diffusive process where the diffusivity depends on r (i.e. $K_r(r)$). In the present case, pairs with small r_0 had multiplied their separation distance within the range of our measurement and therefore had increased their rate of separation, leading to the super-diffusive scaling $\beta > 2$. In contrast, for the largest r_0 case there was $\langle r^2 \rangle^{1/2}/r_0 \approx 1$ for the entire range of our measurements. Therefore, in Richardson's diffusive framework, these pairs had an almost constant diffusivity, so the scaling exponent was $\beta \approx 1$, as expected in a diffusive process with constant diffusivity.

We support the above picture by estimating diffusivity directly. Following Batchelor (1952), we define

$$K_r(r) \equiv \frac{1}{2}\frac{\partial \langle r^2 \rangle}{\partial t}. \tag{4.5}$$

In figure 10(*a*) the diffusivity is plotted against the r.m.s. $\tilde{r} \equiv \langle r^2 \rangle^{1/2}$, where the axes are normalized using the dissipation scales, η and τ_η. An arrow on the figure indicates the direction in which the time grows. For all cases shown, K_r is initially negative, which, as was discussed by Pumir, Shraiman & Chertkov (2001), is a consequence of the negative skewness of the Eulerian velocity differences, aka the 4/5 law (Monin & Yaglom 1972). With increasing time, K_r grows. At small times, K_r grows in line with the ballistic regime,

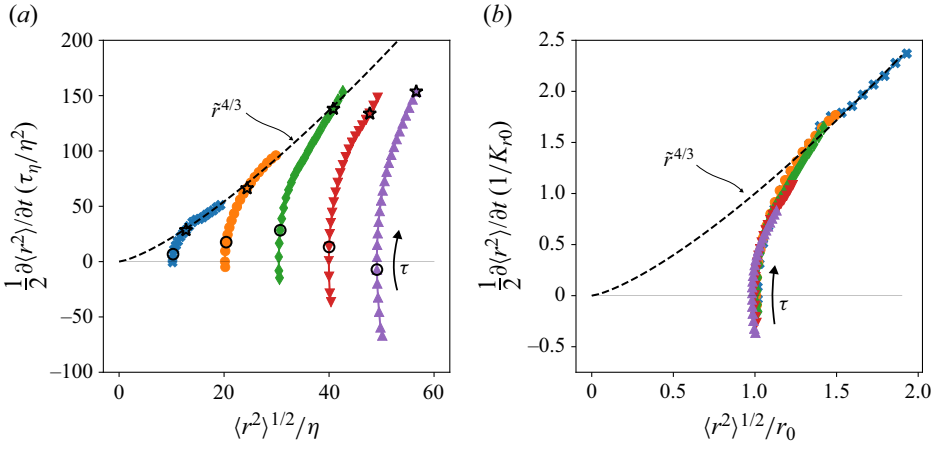

Figure 10. The diffusivity of pair dispersion defined as in (4.5) for various r_0 cases, plotted against the r.m.s. of the separation distance; (*a*) data normalized by dissipation scales and (*b*) by inertial range scaling. Dashed lines correspond to the 4/3s law scaling, (1.2).

the end of which, at $\tau = 0.2\tau_0$, is indicated as circles on the figure. Later on, at $\tau \approx \tau_0$, the separation velocity became decorrelated, which is followed by the inertial regime. The time $\tau = \tau_0$ is indicated by stars on the figure. The range of our measurement extended to this regime ($\tau \gtrsim \tau_0$) for the cases of small r_0.

In the inertial regime, most pronounced for the small r_0 cases, the curves tend to the right side, meaning that as $\tilde{r}$ increased, the diffusivity increased as well. This is the main mechanism leading to the accelerating pair-dispersion picture. Furthermore, the Richardson 4/3 law (as interpreted for the averaged separation by Batchelor 1952), according to (1.2) predicts that $K_r \propto \tilde{r}^{4/3}$. The prediction (1.2) is plotted in the figure as a dashed black line. The data for the two smallest r_0 cases lean towards the dashed line for $\tau > \tau_0$. This observation agrees with previous results that showed a super-diffusive, t^3 scaling range for small initial separations in HIT (Elsinga *et al.* 2021; Tan & Ni 2022).

The Kolmogorov scaling for the diffusivity in the inertial range is $K_r \sim (\tilde{r}^4\epsilon)^{1/3}$. Therefore, we annotate $K_{r_0} \equiv (r_0^4\,\epsilon)^{1/3}$. Accordingly, in figure 10(*b*) the same data are plotted where the axes are normalized using r_0 and K_{r_0}. The data from all r_0 cases are seen to collapse on a single curve under this normalization. The collapse of the data from all r_0 in figure 10(*b*) confirms the existence of a scale-dependent regime in our pair-dispersion measurement. This is a key result of this work. Also, as before, the data for the smallest r_0 case join the $K_r = K_{r_0}(\tilde{r}^4\epsilon)^{1/3}$ line, which corresponds to Richardson's 4/3 law, (1.2). These observations extend the fundamental phenomenology of turbulent pair dispersion to small-scale separation in highly turbulent anisotropic flows.

5. Discussion and conclusions

Our work presents the first empirical investigation of turbulent pair dispersion in a canopy flow. For the analysis, we have used an extensive dataset of Lagrangian trajectories measured in a wind-tunnel experiment using an extended 3D-PTV method (Shnapp *et al.* 2019).

The first part of our analysis focused on the anisotropy of pair dispersion. Our investigation is focused on small scales, being of the order of the separation between canopy obstacles. As opposed to the anisotropy of canopy flow in larger scales, our

measurements show that in the canopy, at the scales of separation between canopy obstacles, pair-dispersion anisotropy is weak. The disparity among the separation components reached only up to approximately 20 % of the total separation. This was the result of our measurements being focused on scales smaller than L_Γ – the scale that determines the cross-over between small-scale local isotropy and large-scale anisotropy (Celani *et al.* 2005). In addition, the time range of our measurement was smaller than Γ^{-1}, so even though particles separate with time and the scales to which they are exposed grow, their separation was still insufficiently large for anisotropy to build up and become prominent.

The weak anisotropy that does exist was observed to grow with time and initial separation. Furthermore, the spanwise dispersion inside the canopy was observed to be the strongest contributor to anisotropy in our measurements, presumably due to flow channelling in between the roughness obstacles. Investigating the pair-dispersion tensor in a framework analogous to the return to isotropy (Lumley & Newman 1977; Stiperski *et al.* 2021) (figure 5), showed that the anisotropy trajectories of pair dispersion progress towards anisotropy on a path that approximates oblate spheroids. Interestingly, in a recent meta-analysis of the Reynolds stress tensors anisotropy trajectories across numerous surface layer flows, a similar trajectory along the oblate topology was observed (Stiperski *et al.* 2021). This similarity might hint that theory developed in the framework of 'return to isotropy' could provide helpful information on pair-dispersion modelling in anisotropic flows; however, this is left for future work.

An important feature observed in our experiments was the smallness of turbulence scales compared with those of mean shear. Due to this feature, the locally isotropic turbulent fluctuations were sufficiently strong to drive the nearly isotropic pair dispersion. This highlights the importance of L_Γ/η and $T_L\Gamma$ to understanding pair dispersion in anisotropic turbulent flows, as having high and low values respectively implies that the isotropic turbulence phenomenology is the appropriate tool for analysis.

The second part of our analysis focused on the two initial regimes of pair dispersion, the ballistic and the inertial, using the conceptual framework of local isotropy. At short times, the particles follow ballistic trajectories with separation velocities dictated by the Eulerian structure function, as observed in homogeneous turbulence (Bourgoin *et al.* 2006). At later times, the separation velocity undergoes decorrelation and a so-called inertial regime ensues. The rate of separation was shown to depend on the scale, r. For pairs with small initial separations, the separation rate was seen to scale in accordance to Richardson's 4/3 law ($r_0 = 10\eta$), in agreement with previous observations in isotropic turbulence (Elsinga *et al.* 2021; Tan & Ni 2022). These observations confirm that the leading mechanisms that govern pair dispersion at small scales in canopy flows are inherently tied to the internal turbulence regulation where the kinetic energy grows with the scale.

The local isotropy in pair dispersion observed in our canopy flow holds due to the focus of our measurements on relatively small scales, $r \ll H$ and $r < L_\Gamma$. At longer times we expect the local isotropy to break and that other mechanisms will become dominant. In particular, although inaccessible in our current dataset, we expect three phenomena to be important at longer times and larger separations. First, the strong shear above the canopy ($z > H$) is expected to make the streamwise component of the separation in this region faster than the vertical and lateral components, thus making pair dispersion at longer times highly anisotropic. This shear dominated regime, characterized by a $r \sim t^{3/2}$ scaling (Monin & Yaglom 1972), was observed in numerical simulations of homogeneous sheared turbulence and channel flows (Shen & Yeung 1997; Pitton *et al.* 2012; Polanco *et al.* 2018), and is expected to occur also above canopy flows for $r \gg L_\Gamma$, according

to the theory of Celani *et al.* (2005). Second, inside the canopy layer ($z < H$) the flow pattern can be very intricate with re-circulation regions behind the roughness elements and a channelling effect of strong flows along certain paths; this complex flow structure has a strong effect on scalar dispersion (Nosek *et al.* 2016; Castro *et al.* 2017; Monnier *et al.* 2018). We expect that these flow patterns will become increasingly dominant in pair-dispersion statistics inside the canopy for separations of the order of the roughness obstacle widths $r \sim W$ (in our canopy $W = \frac{1}{2}H$). In our measurements, only the first approach towards this regime can be noticed in figure 5. Lastly, at scales much larger than the size of the canopy obstacles, $r \ggg H$, yet still inside the canopy, $z < H$, it could be expected that pair dispersion will be dominated by the random passage of the flow in between the roughness obstacles in an analogy to porous medium flow (Brenner 1980); this mechanical diffusion phenomenology (Nepf 1999) would lead to a dispersion regime with a pore scale equal to the obstacle spacing. Notably, for the time being these regimes remain a speculation intended to motivate future studies on this topic, as there are no previous pair-dispersion measurements in canopy flows at these scales.

Understanding pair dispersion is important for modelling dispersion in the environment, as it can be used to estimate the variance of passive scalar concentration fields from known sources. In particular, Cohen & Reynolds (2000), proposed a Lagrangian stochastic modelling approach for pair dispersion in highly inhomogeneous turbulent flows such as canopy flows. Their approach is consistent with the necessary conditions introduced by Thomson (1990), and their model was shown to agree with the experimental results of a scalar released from a known source. Their model also uses the hypothesis that in highly inhomogeneous flows the correlation function for relative velocities is 'short'. In our measurements of the correlation function (figure 8), we show explicitly at what time lag values this hypothesis is valid. In particular, $\rho_{v_\parallel} = 0$ is reached for all tested initial separations at approximately $\tau \approx \tau_0$ (figure 8). This suggests that the concentration variance can be estimated from Cohen and Reynolds dispersion model for times $\tau > \tau_{v_\parallel} \approx \tau_b = (r_0^2/\epsilon)^{1/3}$.

Lastly, it is important to regard our interpretation of the results using Richardson's turbulent diffusivity framework. Indeed, turbulent pair dispersion is an intermittent process (Boffetta & Sokolov 2002*b*; Bitane *et al.* 2012; Scatamacchia *et al.* 2012; Shnapp & Liberzon 2018; Tan & Ni 2022), and this characteristic cannot be described using the diffusivity model since it precludes longer correlation times. Nevertheless, as this is the first empirical investigation of the topic in a canopy flow, it is of particular importance to lay out the leading mechanisms that govern the phenomenon, which include the growth of the kinetic energy with the scale. Since the diffusivity framework lends itself somewhat naturally to the description of this phenomenology, it is the one that was chosen. With this, the treatment of more refined characteristics of pair dispersion at small scales is left for future research. To that should be added the treatment of pair dispersion over larger scales, which could not have been examined using the presently available dataset.

Acknowledgements. We are grateful to M. Konn, S. Kalenko, G. Gulitski, V. Babin, A. Shick and M. Hotovely, for their assistance in the wind-tunnel experiment.

Funding. This study is supported by the PAZY grants 2403170 and 1372020.

Declaration of interests. The authors report no conflict of interest.

Author ORCIDs.
Ron Shnapp https://orcid.org/0000-0001-7495-8420;
Alex Liberzon https://orcid.org/0000-0002-6882-4191.

Appendix. Subvolume flow parameters

sv	$\tilde{u}$ (m s^{-1})	ϵ (W kg^{-1})	η (mm)	τ_η (s)	λ (mm)	Re_λ	H/η
$a1$	0.42	0.201	0.36	0.009	14.14	398	277
$a2$	0.45	0.256	0.34	0.008	13.25	394	295
$a3$	0.49	0.304	0.32	0.007	13.23	428	308
$a4$	0.51	0.244	0.34	0.008	15.35	517	291
$a5$	0.62	0.239	0.34	0.008	19.01	784	290
$b1$	0.36	0.123	0.41	0.011	15.41	369	245
$b2$	0.42	0.193	0.36	0.009	14.18	392	275
$b3$	0.47	0.250	0.34	0.008	14.09	440	293
$b4$	0.50	0.233	0.35	0.008	15.63	523	288
$b5$	0.65	0.305	0.32	0.007	17.63	762	308
$c1$	0.42	0.248	0.34	0.008	12.59	350	292
$c2$	0.43	0.210	0.36	0.008	13.97	397	280
$c3$	0.46	0.286	0.33	0.007	12.82	390	303
$c4$	0.52	0.231	0.35	0.008	16.13	555	287
$c5$	0.62	0.245	0.34	0.008	18.66	766	291
$d1$	0.40	0.175	0.37	0.009	14.18	373	268
$d2$	0.40	0.175	0.37	0.009	14.32	380	268
$d3$	0.47	0.229	0.35	0.008	14.61	454	287
$d4$	0.50	0.218	0.35	0.008	15.99	530	283
$d5$	0.66	0.377	0.31	0.006	16.10	707	325

Table 1. Turbulence parameters for each sub-volume for the $Re_\infty = 16 \times 10^3$ case.

sv	$\tilde{u}$ (m s^{-1})	ϵ (W kg^{-1})	η (mm)	τ_η (s)	λ (mm)	Re_λ	H/η
$a1$	0.53	0.422	0.30	0.006	12.16	426	334
$a2$	0.54	0.551	0.28	0.005	11.01	399	357
$a3$	0.60	0.703	0.26	0.005	10.68	424	379
$a4$	0.64	0.611	0.27	0.005	12.19	516	366
$a5$	0.83	0.669	0.27	0.005	15.19	839	375
$b1$	0.47	0.257	0.34	0.008	13.80	429	295
$b2$	0.50	0.352	0.31	0.007	12.74	427	319
$b3$	0.60	0.497	0.29	0.005	12.83	516	348
$b4$	0.64	0.487	0.29	0.006	13.79	589	346
$b5$	0.75	0.544	0.28	0.005	15.17	754	356
$c1$	0.52	0.490	0.29	0.006	11.05	379	347
$c2$	0.53	0.412	0.30	0.006	12.46	442	332
$c3$	0.60	0.587	0.28	0.005	11.68	464	363
$c4$	0.64	0.565	0.28	0.005	12.79	546	359
$c5$	0.81	0.706	0.26	0.005	14.49	783	380
$d1$	0.53	0.371	0.31	0.006	13.03	459	323
$d2$	0.52	0.327	0.32	0.007	13.72	478	313
$d3$	0.59	0.524	0.28	0.005	12.28	485	353
$d4$	0.63	0.528	0.28	0.005	12.94	540	353
$d5$	0.88	0.876	0.25	0.004	14.13	830	401

Table 2. Turbulence parameters for each sub-volume for the $Re_\infty = 26 \times 10^3$ case.

Tables 1 and 2 present the flow parameters used in the calculations for each of the sub-volumes. Detailed calculations of these properties are given in Shnapp *et al.* (2020).

References

Arnèodo, A., *et al.* 2008 Universal intermittent properties of particle trajectories in highly turbulent flows. *Phys. Rev. Lett.* **100**, 254504.

Aylor, D.E. & Flesch, T.K. 2001 Estimating spore release rates using a Lagrangian stochastic simulation model. *J. Appl. Meteorol.* **40** (7), 1196–1208.

Bailey, B.N., Stoll, R. & Pardyjak, E.R. 2018 A theoretically consistent framework for modelling Lagrangian particle deposition in plant canopies. *Boundary-Layer Meteorol.* **167** (3), 509–520.

Baldocchi, D. 1997 Flux footprints within and over forest canopies. *Boundary-Layer Meteorol.* **85** (2), 273–292.

Batchelor, G.K. 1952 Diffusion in a field of homogeneous turbulence: II. The relative motion of particles. *Math. Proc. Camb. Phil. Soc.* **48** (2), 345–362.

Belcher, S.E. 2005 Mixing and transport in urban areas. *Phil. Trans. R. Soc.* **363**, 2947–2968.

Berg, J., Lüthi, B., Mann, J. & Ott, S. 2006 Backwards and forwards relative dispersion in turbulent flow: an experimental investigation. *Phys. Rev.* E **74**, 016304.

Biferale, L., Bodenschatz, E., Cencini, M., Lanotte, A.S., Ouellette, N.T., Toschi, F. & Xu, H. 2008 Lagrangian structure functions in turbulence: a quantitative comparison between experiment and direct numerical simulation. *Phys. Fluids* **20** (6), 065103.

Biferale, L., Boffetta, G., Celani, A., Devenish, B.J., Lanotte, A. & Toschi, F. 2005 Lagrangian statistics of particle pairs in homogeneous isotropic turbulence. *Phys. Fluids* **17** (11), 115101.

Biferale, L., Lanotte, A.S., Scatamacchia, R. & Toschi, F. 2014 Intermittency in the relative separations of tracers and of heavy particles in turbulent flows. *J. Fluid Mech.* **757**, 550–572.

Bitane, R., Homann, H. & Bec, J. 2012 Time scales of turbulent relative dispersion. *Phys. Rev.* E **86**, 045302.

Boffetta, G. & Sokolov, I.M. 2002*a* Relative dispersion in fully developed turbulence: the Richardson's law and intermittency corrections. *Phys. Rev. Lett.* **88**, 094501.

Boffetta, G. & Sokolov, M. 2002*b* Statistics of two-particle dispersion in two-dimensional turbulence. *Phys. Fluids*, 3224–3232.

Bohbot-Raviv, Y., Shnapp, R., Liberzon, A., Babin, V., Hotoveli, M., Shick, A. & Fattal, E. 2017 Turbulence statistics of canopy-flows using novel Lagrangian measurements within an environmental wind tunnel. In *Physmod*. LHEEA-DAUC, Ecole Centrale de Nantes.

Bourgoin, M. 2015 Turbulent pair dispersion as a ballistic cascade phenomenology. *J. Fluid Mech.* **772**, 678–704.

Bourgoin, M., Ouellette, N.T., Xu, H., Berg, J. & Bodenschatz, E. 2006 The role of pair dispersion in turbulent flow. *Science* **311**, 835–838.

Brenner, H. 1980 Dispersion resulting from flow through spatially periodic porous media. *Phil. Trans. R. Soc. Lond. Ser.* A *Math. Phys. Sci.* **297** (1430), 81–133.

Britter, R.E. & Hanna, S.R. 2003 Flow and dispersion in urban areas. *Annu. Rev. Fluid Mech.* **35**, 469–496.

Brunet, Y. 2020 Turbulent flow in plant canopies: historical perspective and overview. *Boundary-Layer Meteorol.* **177**, 315–364.

Brunet, Y., Finnigan, J.J. & Raupach, M.R. 1994 A wind tunnel study of air flow in waving wheat: single-point velocity statistics. *Boundary-Layer Meteorol.* **70** (1), 95–132.

Casciola, C., Gualtieri, P., Benzi, R. & Piva, R. 2003 Scale-by-scale budget and similarity laws for shear turbulence. *J. Fluid Mech.* **476**, 105–114.

Castro, I.P., Xie, Z.-T., Fuka, V., Robins, A.G., Carpentieri, M., Hayden, P., Hertwig, D. & Coceal, O. 2017 Measurements and computations of flow in an urban street system. *Boundary-Layer Meteorol.* **162**, 207–230.

Celani, A., Cencini, M., Vergassola, M., Villermaux, E. & Vincenzi, D. 2005 Shear effects on passive scalar spectra. *J. Fluid Mech.* **523**, 99–108.

Cohen, J.E. & Reynolds, A.M. 2000 Parameterization of the two-point velocity correlation function in a two-particle Lagrangian stochastic model and its effect on the prediction of concentration variances due to a line source. *J. Appl. Meteorol. Climatol.* **39**, 1762–1769.

DePaul, F.T. & Sheih, C.M. 1986 Measurements of wind velocities in a street canyon. *Atmos. Environ.* **20** (3), 455–459.

Dracos, T. 1996 *Three-Dimensional Velocity and Vorticity Measuring and Image Analysis Technique*. Lecture Notes from the short course held in Zurich, Switzerland. Kluwer Academic Publisher.

Duman, T., Trakhtenbrot, A., Poggi, D., Cassiani, M. & Katul, G.G. 2016 Dissipation intermittency increases long-distance dispersal of heavy particles in the canopy sublayer. *Boundary-Layer Meteorol.* **159** (1), 41–68.

ELSINGA, G.E., ISHIHARA, T. & HUNT, J.C.R. 2021 Non-local dispersion and the reassessment of Richardson's t^3-scaling law. *J. Fluid Mech.* **932**, A17.

FALKOVICH, G., GAWĘDZKI, K. & VERGASSOLA, M. 2001 Particles and fields in fluid turbulence. *Rev. Mod. Phys.* **73**, 913–975.

FATTAL, E., DAVID-SAROUSSI, H., BUCHMAN, O., TAS, E. & KLAUSNER, Z. 2023 Heterogenous canopy in a Lagrangian-Stochastic dispersion model for particulate matter from multiple sources over the Haifa Bay Area. *Atmosphere* **14** (1), 144.

FATTAL, E., DAVID-SAROUSSI, H., KLAUSNER, Z. & BUCHMAN, O. 2021 An urban Lagrangian stochastic dispersion model for simulating traffic particulate-matter concentration fields. *Atmosphere* **12** (5), 580.

FINNIGAN, J. 2000 Turbulence in plant canopies. *Annu. Rev. Fluid Mech.* **32**, 519–571.

GHISALBERTI, M. & NEPF, H.M. 2002 Mixing layers and coherent structures in vegetated aquatic flows. *J. Geophys. Res.: Oceans* **107** (C2), 3011.

KATUL, G., OREN, R., ELLSWORTH, D., HSIEH, C.I. & PHILLIPS, N. 1997 A Lagrangian dispersion model for predicting co_2 sources, sinks, and fluxes in a uniform loblolly pine. *J. Geophys. Res.* **102** (D8), 9309–9321.

KIM, J.-T. & CHAMORRO, L.P. 2019 Lagrangian description of the unsteady flow induced by a single pulse of a jellyfish. *Phys. Rev. Fluids* **4**, 064605.

KOLMOGOROV, A.N. 1941 The local structure of turbulence in incompressible viscous fluid for very large Reynolds numbers. *C. R. Acad. Sci. URSS* **30**, 301–305.

LIOT, O., MARTIN-CALLE, D., GAY, A., SALORT, J., CHILLÀ, F. & BOURGOIN, M. 2019 Pair dispersion in inhomogeneous turbulent thermal convection. *Phys. Rev. Fluids* **4**, 094603.

LUMLEY, J.L. & NEWMAN, G.R. 1977 The return to isotropy of homogeneous turbulence. *J. Fluid Mech.* **82** (1), 161–178.

LUTHI, B., TSINOBER, A. & KINZELBACH, W. 2005 Lagrangian measurment of vorticity dynamics in turbulent flow. *J. Fluid Mech.* **528**, 87–118.

MALIK, N.A., DRACOS, T. & PAPANTONIOU, D.A. 1993 Particle tracking velocimetry in three-dimensional flows part II: particle tracking. *Exp. Fluids* **15**, 279–294.

MASS, H.G., GRUEN, D. & PAPANTONIOU, D. 1993 Particle tracking velocimetry in three-dimensional flows part I: photogrammetric determination of particle coordinates. *Exp. Fluid* **15**, 133–146.

MELLER, Y. & LIBERZON, A. 2016 Particle data management software for 3D particle tracking velocimetry and related applications – the flowtracks package. *J. Open Res. Softw*. 23.

MONIN, A.S. & YAGLOM, A.M. 1972 *Statistical Fluid Mechanics*. Dover Publications.

MONNIER, B., GOUDARZI, S.A., VINUESA, R. & WARK, C. 2018 Turbulent structure of a simplified urban fluid flow studied through stereoscopic particle image velocimetry. *Boundary-Layer Meteorol.* **166**, 239–268.

NEPF, H.M. 1999 Drag, turbulence, and diffusion in flow through emergent vegetation. *Water Resour. Res.* **35** (2), 479–489.

NI, R. & XIA, K.Q. 2013 Experimental investigation of pair dispersion with small initial separation in convective turbulent flows. *Phys. Rev.* E **87**, 063006.

NOSEK, S., Kukacka, L., Kellnerova, R., Jurcakova, K. & Janour, Z. 2016 Ventilation processes in a three-dimensional street canyon. *Boundary-Layer Meteorol.* **159**, 259–284.

OPENPTV CONSORTIUM 2014 Open source particle tracking velocimetry. https://www.openptv.net.

OTT, S. & MANN, J. 2000 An experimental investigation of the relative diffusion of particle pairs in three-dimensional turbulent flow. *J. Fluid Mech.* **422**, 207–223.

OUELLETTE, N.T., XU, H., BOURGOIN, M. & BODENSCHATZ, E. 2006*a* Small-scale anisotropy in Lagrangian turbulence. *New J. Phys.* **8**, 102.

OUELLETTE, N.T., XU, H., BOURGOIN, M. & BODENSCHATZ, E. 2006*b* An experimental study of turbulent relative dispersion models. *New J. Phys.* **8**, 109.

PITTON, E., MARCHIOLI, C., LAVEZZO, V., SOLDATI, A. & TOSCHI, F. 2012 Anisotropy in pair dispersion of inertial particles in turbulent channel flow. *Phys. Fluids* **24** (7), 073305.

POGGI, D., KATUL, G. & ALBERTSON, J. 2006 Scalar dispersion within a model canopy: measurements and three-dimensional Lagrangian models. *Adv. Water Resour.* **29** (2), 326–335.

POLANCO, J.I. 2019 Lagrangian properties of turbulent channel flow: a numerical study. PhD thesis, l'Université Claude Bernard Lyon 1.

POLANCO, J.I., VINKOVIC, I., STELZENMULLER, N., MORDANT, N. & BOURGOIN, M. 2018 Relative dispersion of particle pairs in turbulent channel flow. *Intl J. Heat Fluid Flow* **71**, 231–245.

POPE, S.B. & CHEN, Y.L. 1990 The velocity-dissipation probability density function model for turbulent flows. *Phys. Fluids* A*: Fluid Dyn.* **2** (8), 1437–1449.

PUMIR, A., SHRAIMAN, B.I. & CHERTKOV, M. 2001 The Lagrangian view of energy transfer in turbulent flow. *Europhys. Lett*. **56**, 379.

RAST, M.P. & PINTON, J.-F. 2011 Pair dispersion in turbulence: the subdominant role of scaling. *Phys. Rev. Lett.* **107**, 214501.

RAUPACH, M.R. 1987 A Lagrangian analysis of scalar transfer in vegetation canopies. *Q. J. R. Meteorol. Soc.* **113**, 107–120.

RAUPACH, M.R., FINNIGAN, J.J. & BRUNET, Y. 1996 Coherent eddies and turbulence in vegetative canopies: the mixing-layer analogy. *Boundary-Layer Meteorol.* **78**, 351–382.

RAUPACH, M.R. & THOM, A.S. 1981 Turbulence in and above plant canopies. *Annu. Rev. Fluid Mech.* **13** (1), 97–129.

REYNOLDS, A.M. 1998 On the formulation of Lagrangian stochastic models of scalar dispersion within plant canopies. *Boundary-Layer Meteorol.* **86** (2), 333–344.

RICHARDSON, L.F. 1926 Atmospheric diffusion shown on a distance-neighbour graph. *Proc. R. Soc. Lond. Ser.* A *Contain. Pap. Math. Phys. Character* **110** (756), 709–737.

SALAZAR, J.P.L.C. & COLLINS, L.R. 2009 Two-particle dispersion in isotropic turbulent flows. *Annu. Rev. Fluid Mech.* **41** (1), 405–432.

SAWFORD, B. 2001 Turbulent relative dispersion. *Annu. Rev. Fluid Mech.* **33** (1), 289–317.

SCATAMACCHIA, R., BIFERALE, L. & TOSCHI, F. 2012 Extreme events in the dispersions of two neighboring particles under the influence of fluid turbulence. *Phys. Rev. Lett.* **109**, 144501.

SCHUMACHER, J. 2008 Lagrangian dispersion and heat transport in convective turbulence. *Phys. Rev. Lett.* **100**, 134502.

SHARMA, G. & PHARES, D.J. 2006 Turbulent transport of particles in a straight square duct. *Intl J. Multiphase Flow* **32** (7), 823–837.

SHEN, P. & YEUNG, P.K. 1997 Fluid particle dispersion in homogeneous turbulent shear flow. *Phys. Fluids* **9** (11), 3472–3484.

SHIG, L., BABIN, V., SHNAPP, R., FATTAL, E., LIBERZON, A. & BOHBOT-RAVIV, Y. 2023*a* Flow and turbulence statistics of a two-height canopy model in a wind tunnel. *Boundary-Layer Meteorol*. 591–617.

SHIG, L., BABIN, V., SHNAPP, R., FATTAL, E., LIBERZON, A. & BOHBOT-RAVIV, Y. 2023*b* Quadrant analysis of the reynolds shear stressin a two-height canopy. *Flow Turbul. Combust*. 35–57.

SHNAPP, R. 2021 On small-scale and large-scale intermittency of Lagrangian statistics in canopy flow. *J. Fluid Mech.* **913**, R2.

SHNAPP, R., BOHBOT-RAVIV, Y., LIBERZON, A. & FATTAL, E. 2020 Turbulence-obstacle interactions in the Lagrangian framework: applications for stochastic modeling in canopy flows. *Phys. Rev. Fluids* **5**, 094601.

SHNAPP, R., BRIZZOLARA, S., NEAMTU-HALIC, M.M., GAMBINO, A. & HOLZNER, M. 2023 Universal alignment in turbulent pair dispersion. *Nat. Commun.* **14** (1), 4195.

SHNAPP, R. & LIBERZON, A. 2018 Generalization of turbulent pair dispersion to large initial separations. *Phys. Rev. Lett.* **120**, 244502.

SHNAPP, R., SHAPIRA, E., PERI, D., BOHBOT-RAVIV, Y., FATTAL, E. & LIBERZON, A. 2019 Extended 3D-PTV for direct measurements of Lagrangian statistics of canopy turbulence in a wind tunnel. *Sci. Rep.* **9**, 7405.

SOKOLOV, I.M., KLAFTER, J. & BLUMEN, A. 2000 Ballistic versus diffusive pair dispersion in the Richardson regime. *Phys. Rev.* E **61**, 2717–2722.

SREENIVASAN, K.R. 1995 On the universality of the Kolmogorov constant. *Phys. Fluids* **7**, 2778–2784.

STIPERSKI, I., KATUL, G.G. & CALAF, M. 2021 Universal return to isotropy of inhomogeneous atmospheric boundary layer turbulence. *Phys. Rev. Lett.* **126** (19), 194501.

TAN, S. & NI, R. 2022 Universality and intermittency of pair dispersion in turbulence. *Phys. Rev. Lett.* **128** (11), 114502.

TAYLOR, G.I. 1922 Diffusion by continuous movements. In *Proceedings of the London Mathematical Society*. Wiley.

THALABARD, S., KRSTULOVIC, G. & BEC, J. 2014 Turbulent pair dispersion as a continuous-time random walk. *J. Fluid Mech.* **755**, 4.

THOMSON, D.J. 1987 Criteria for the selection of stochastic models of particle trajectories in turbulent flows. *J. Fluid Mech.* **180**, 529–556.

THOMSON, D.J. 1990 A stochastic model for the motion of particle pairs in isotropic high-Reynolds-number turbulence, and its application to the problem of concentration variance. *J. Fluid Mech.* **210**, 113–153.

WILSON, J.D., YEE, E., EK, N. & D'AMOURS, R. 2009 Lagrangian simulation of wind transport in the urban environment. *Q. J. R. Meteorol. Soc.* **135** (643), 1586–1602.

YEUNG, P.K. 1994 Direct numerical simulation of two-particle relative diffusion in isotropic turbulence. *Phys. Fluids* **6** (10), 3416–3428.